MADRID
inter.noise 2019
June 16 - 19
NOISE CONTROL FOR A BETTER ENVIRONMENT

Numerical prediction of the far field noise generated by a ship propeller

Marta Cianferra[1]
University of Trieste
Dipartimento di Ingegneria e Architettura,
via Alfonso Valerio 10, I-34127 Trieste, Italy

Vincenzo Armenio[2]
University of Trieste
Dipartimento di Ingegneria e Architettura,
via Alfonso Valerio 10, I-34127 Trieste, Italy

Andrea Petronio[3]
Iefluids S.r.l.,
Piazzale Europa 1, I-34127 Trieste, Italy

ABSTRACT

Our research focuses on assessment and use of mathematical and numerical models for the characterization of the noise source, when the noise is generated by a fluid in motion around a body. In particular, within the framework of the acoustic analogy, we first evaluate the fluid dynamic field using Large-Eddy Simulation (LES) and then we apply the Ffowcs-Williams and Hawkings (FWH) equation to reconstruct the acoustic field. First we show the conditions under which the non-linear terms of the FWH equation can be computed by direct integration neglecting the compressible delay in the volume integral terms. Successively we evaluate the noise generated by simple, still significant, geometries, and finally we consider noise propagation from a ship propeller in uniform flow. For the latter we observe the tonal signal given by the blade rotational frequency together with a high amplitude broadband noise given by the wake.

Keywords: Hydroacoustics, Ship propeller, Ffowcs Williams and Hawkings
I-INCE Classification of Subject Number: 76

[1]marta.cianferra@phd.units.it
[2]vincenzo.armenio@dia.units.it
[3]andrea.petronio@gmail.com

1. INTRODUCTION

Analysis of fluid mechanics noise is of primary importance in a number of industrial and environmental applications.

In hydrodynamics, the new concept of silent ship, for reducing the environmental impact, requires the development of new and state-of-art methodologies.

The effect on the far-field noise of a persistent wake in hydrodynamics is more relevant and important than in aeroacoustics. This is the reason for which most research in hydroacoustic is oriented toward development of models for an accurate reproduction of the quadrupole terms coming from the wake.

The Ffowcs Williams and Hawkings (FWH) equation has become a widely used method to reconstruct the acoustic field from the fluid dynamic data. The integral formulation (solution of a non homogeneous wave equation) allows the evaluation of the acoustic field through a relatively simple post-processing of fluid dynamic data. An important feature is the relationship between the resulting acoustic pressure and three different integral terms (corresponding to three different source terms of the FW-H differential equation), which are representative of all possible noise generation mechanisms. Two terms correspond to surface (hereafter referred to as *linear terms*) integrals and identify two processes: the noise generated by the fluid displaced by the body (thickness component) and that coming from the fluid dynamic loads acting on the body surface (loading component). The third term of the FWH equation accounts for all possible sources occurring in the fluid, such as turbulence, vorticity, etc.; it is known as the *nonlinear terms* of the FWH equation (or quadrupole noise) and, requires a volume integration over the whole fluid region affected by the fluid motion.

The direct evaluation of such nonlinear term has been carried out rarely, for many years the quadrupole noise was believed to be irrelevant.

But recent literature [1] has demonstrated the importance of the nonlinear quadrupole terms in the far field noise propagation for a wide class of engineering problems; however, still the direct integration of the volume terms has been avoided for a series of problems, the most important being the evaluation of the time-delay which makes the numerical computation impractical. This aspect was addressed in [2], where a non dimensional parameter, related to length and time scale of the problem, justify the omission of time delays computation.

As regards the fluid-dynamic field to be used as input data for the acoustic analysis, in literature it has been well recognize that the quality of the data plays a very important role (for a discussion see the review paper of Brentner and Farassat [3]). In recent works (see among others [1]) the hydroacoustic behavior of a marine propeller was studied combining a RANS simulation with the FWH porous method; a common observation states the inadequacy of a RANS approach to capture the nonlinear noise sources, required to achieve an accurate noise prediction.

In the present work, we adopt LES to reproduce, first flow around bluff bodies and then, an isolated marine propeller in uniform flow. The former case was necessary to assess the acoustic method and understand the contribution of the various FWH terms. The latter simulation is a case of practical interest on which the acoustic model can be correctly exploited.

2. MATHEMATICAL MODEL

2.2.1. Fluid dynamic model

We use LES, in which the large anisotropic and energy-carrying scales of motion are directly resolved through an unsteady and 3D simulation, whereas the more isotropic and dissipative small scales of motion are confined in the sub-grid space. Scale separation is carried out through a filtering operation of the flow variables.

Since we investigate both flow around bluff bodies and isolated marine propeller, to enclose all the cases, we report the incompressible Navier-Stokes equations, formulated for the absolute velocity vector in case of a rotating reference system, as proposed in [4], with the Coriolis and centrifugal body forces that take into account the rotational effects, along with the continuity equation:

$$\frac{\partial \overline{u}_i}{\partial x_i} = 0, \tag{1}$$

$$\frac{\partial \overline{u}_i}{\partial t} + \frac{\partial}{\partial x_j}\left(\overline{u}_i\overline{u}_j - \overline{u}_i\epsilon_{jkl}\omega_k x_l\right) = \frac{\partial \overline{p}}{\partial x_i} - \epsilon_{ijk}\omega_j\overline{u}_k + \nu\frac{\partial^2\overline{u}_i}{\partial x_j\partial x_j} - \frac{\partial \tau_{ij}}{\partial x_j}, \tag{2}$$

where the overbar denotes filtering operation. Filtering is performed implicitly, using the grid cell as top-hat filter in the physical space. In eqs. (1), (2) u_i represents the component of the absolute velocity in the i-direction, p is the kinematic pressure, x_i is the i-component of the Cartesian coordinates in the rotating frame of reference, ω_i is i-component of the angular velocity of rotating frame of reference, and when $\omega_i = 0$, for $i = 1, 2, 3$, the standard equations for inertial reference system are retained. ν is the kinematic viscosity, ϵ_{ijk} is the Levi-Civita tensor, $\tau_{ij} = \left(\overline{u_iu_j} - \overline{u}_i\overline{u}_j\right)$ is the SGS stress tensor, coming from filtering the non-linear terms of the Navier-Stokes equations.

The SGS stress tensor is here modeled using the dynamic Lagrangian model, developed by Meneveau *et al.* [5]. Some more details on the formulation are reported in Cintolesi *et al.* [6,7].

2.2.2. Acoustic model

In presence of a background uniform flow, the acoustic waves are advected by the mean flow. Thus, the integral Ffowcs-Williams and Hawkings equation needs to be considered in the convective form. It is obtained by solving the advective wave equation with the use of the advective Green's function.

The acoustic pressure $\hat{p}$, at any point $\mathbf{x}$ and time t, is represented by the sum of surface ($\hat{p}_{2D}$) and volume integrals ($\hat{p}_{3D}$).

Considering an uniform flow with velocity U_0 along the direction x_1 the surface terms may be written [8] as

$$\begin{aligned} 4\pi\hat{p}_{2D}(\mathbf{x},t) = & \frac{\partial}{\partial t}\int_{f=0}\left[(1-M_0\hat{r}_1)\frac{\rho_0 v_{\hat{n}}}{r^*}\right]_\tau dS - U_0\int_{f=0}\left[\frac{\rho_0 v_{\hat{n}}\hat{r}_1^*}{r^{*2}}\right]_\tau dS \\ & + \frac{1}{c_0}\frac{\partial}{\partial t}\int_{f=0}\left[\frac{L_{ij}\hat{n}_j\hat{r}_i}{r^*}\right]_\tau dS + \int_{f=0}\left[\frac{L_{ij}\hat{n}_j\hat{r}_i^*}{r^{*2}}\right]_\tau dS, \end{aligned} \tag{3}$$

where $v_{\hat{n}}$ is the projection of the body velocity along $\hat{n}$ the outward unit normal vector to the surface element dS, $\hat{r}$ and $\hat{r}^*$ are unit radiation vectors (see next section), the appearance of their first components $\hat{r}_1$ and $\hat{r}_1^*$ is due to the mean flow which advects the pressure acoustic field along the x-axis direction, r and r^* are the module of the radiation vectors $\mathbf{r}$ and $\mathbf{r}^*$ respectively, $M_0 = U_0/c_0$ is the inlet Mach number and c_0 is the sound speed. The tensor L_{ij} appearing in (3) is given by $L_{ij} = [\rho_0 u_i \left(u_j + U_0\delta_{1j} - v_j\right) + P_{ij}]$, where u_i indicates the i component of the fluid perturbation velocity $\mathbf{u}$, $P_{ij} = (p - p_0)\delta_{ij} - \sigma_{ij}$ is the compressive stress tensor, with $p - p_0$ the flow pressure perturbation with respect to the reference value p_0, σ_{ij} the viscous stress tensor and δ_{ij} the Kronecker delta.

The volume integrals are derived in [9] and assume the form

$$\begin{aligned} 4\pi\hat{p}_{3D}(\mathbf{x},t) &= \frac{1}{c_0^2}\frac{\partial^2}{\partial t^2}\int_{f>0}\left\{T_{ij}\left[\frac{\hat{r}_i\hat{r}_j}{r^*}\right]\right\}_\tau dV + \int_{f>0}\left\{T_{ij}\left[\frac{3\hat{r}_i^*\hat{r}_j^* - R_{ij}^*}{r^{*3}}\right]\right\}_\tau dV \\ &+ \frac{1}{c_0}\frac{\partial}{\partial t}\int_{f>0}\left\{T_{ij}\left[\frac{2\hat{r}_i\hat{r}_j^*}{r^{*2}} + \frac{\hat{r}_i^*\hat{r}_j^* - R_{ij}^*}{\beta^2 r^{*2}}\right]\right\}_\tau dV \end{aligned} \tag{4}$$

Equation (4) contains two second–order tensors: R_{ij}^* (for the complete derivation and more details see [9]) and the well known Lighthill stress tensor T_{ij}, characterizing the FW-H quadrupole terms. Under the assumption of negligible viscous effects, constant flow density and iso-entropic transformations for the fluid in the acoustic field, the Lighthill tensor reads as $T_{ij} = \rho_0 u_i u_j + (p - p_0)\delta_{ij}$. The index τ in eqs. (3) and (4) denotes that the integral kernels are computed at the emission (retarded) time

$$\tau = t - r/c_0 = t + \frac{|\mathbf{x}(t) - \mathbf{y}(\tau)|}{c_0}. \tag{5}$$

τ is the instant at which the noise impulse starts at the source point $\mathbf{y}$, to reach the observer $\mathbf{x}$ at the observer time t. The difference between observer and emission time is known as compressibility delay and points out that sound propagates in the fluid at a finite speed and sound waves may add up. A discussion on the importance of the time delay is reported in [2], where a non-dimensional parameter, based on speed of sound, length scale and time scale of the problem, is defined. Also, in presence of a moving body, the retarded surface [10] can be evaluated. This is done in section 4.1 for the case of the ship propeller. In equations 3 and 4 we omitted the term $1 - M_r$ in the denominator of all terms, since the maximum value of $M_r = v_1 r_i/c_0$, at the blade tip, is close to zero.

The function f represents the integration domain. The points in space such that $f(\mathbf{x},t) = 0$ may describe a surface S coincident with the surface of the body–source or, alternatively, a closed (porous) surface S_p, embedding the body together with a fluid region around it, acting as a radiating domain. Since recent studies have demonstrated the drawbacks of the porous formulation (see among others [2,4]) in our study the standard FWH equation is adopted, thus equations 3 and 4 are solved, considering S (the solid surface of the immersed body) and V the volume of fluid where the wake develops. All the results are presented separating the linear (equation 4) and nonlinear (equation 4) terms contribution.

3. FLOW AROUND ELEMENTARY GEOMETRIES

In this Section we summarize the results related to cases previously studied. The flow around bluff bodies was a useful way to approach the acoustic model and to understand some important features related to the sound waves generated by the fluid motion. Indeed, in spite of the geometrical simplification, the study of hydrodynamic noise generated around simple bodies is significant, because it can exploit fundamental aspects of the topology of the flow field which, in turn, rules generation and propagation of hydrodynamic noise. Two mechanisms of noise generation are observed when applying acoustic analogies: the fluid-surface interaction which corresponds to the pressure scattered by the solid surface of the immersed body, and the vortex sound given by the pure flow motion. We observed that the latter, in presence of coherent and organized structures, is an important (or even dominant) noise source, while, the hydrodynamic shape of the body reduces the loads on the frontal area and thus the noise level. Two comparisons are carried out in the following subsections: sphere vs prolate spheroid in 3.1, and cube vs square cylinder in 3.2.

3.3.1. Sphere vs prolate spheroid

In this subsection, uniform flows around a sphere and a prolate spheroid at zero angle of attack are considered. For sake of comparison, the Reynolds number, based on the square root of the reference (frontal) area, the uniform inlet velocity, and the viscosity, is $Re_A = \sqrt{(A)}U_0/\nu = 4430$ for the two objects.

Instantaneous streamtracers in Figure 1 give a qualitative sight of the flow at the rear of the two bodies. Flow separation is substantially different in the two cases. the sphere produces downstream massive separation and a wake characterized by overlapping of vortex shedding and energetic turbulence generated by a shear layer; the separation angle on the sphere is about 90^o; the main recirculation beyond the sphere covers a long region up to $x = 2D$ where the mean flow reattaches, while smaller recirculation spots are present in the proximity of the surface. The prolate spheroid is aligned with the main current, it develops a small separation region in the leading edge region and a slender wake, much less intense than the sphere case, characterized by small vortex.

The FWH reconstructed signal, meaning the acoustic pressure generated by the two bodies, is in Figure 2. The contribution of the linear terms is on the left panel, whereas the contribution of nonlinear terms is on the right panel. The microphone is located at the rear of the body, in order to capture both the loading (linear) and the quadrupole (non-linear) noise, at $100\,D$ far from the body, being D the sphere diameter. It is noticeable how the signal of the bluff body (black dashed line) is richer in frequency and higher in amplitude. Also, it is interesting to look at the respective contributions of linear and non-linear terms in the two cases: for the sphere both loading and quadrupole terms have an amplitude of about $20\,dB$ while the hydrodinamic shape of the prolate spheroid reduces the impact of the surface with the fluid (and therefore the loading noise), but generates a weak vortex shedding that produces low frequency noise. The fact that the acoustic signal is low, (with maximum around $20\,dB$), is due to the fact that the microphone is very far from the noise source and the reference pressure is that of water $p_{ref} = 10^{-6}$, used when computing the logarithmic scale (decibel).

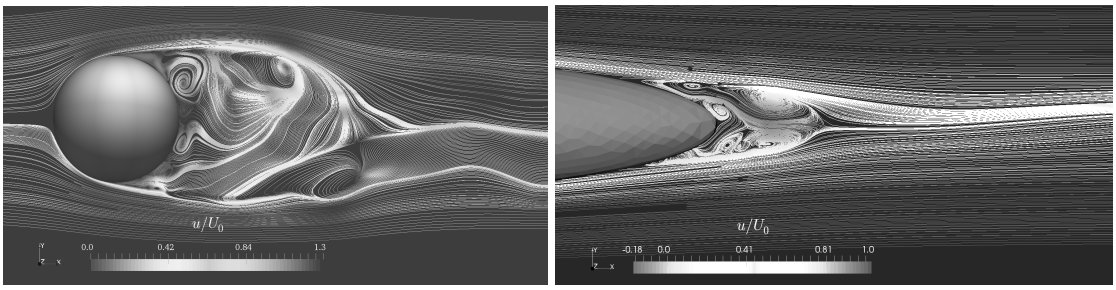

Figure 1: Comparison of instantaneous streamline velocity u, made non-dimensional by the inlet uniform velocity U_0, in the case of flow around a sphere (left panel) and flow around a prolate spheroid (right panel). The Figure was taken from [11].

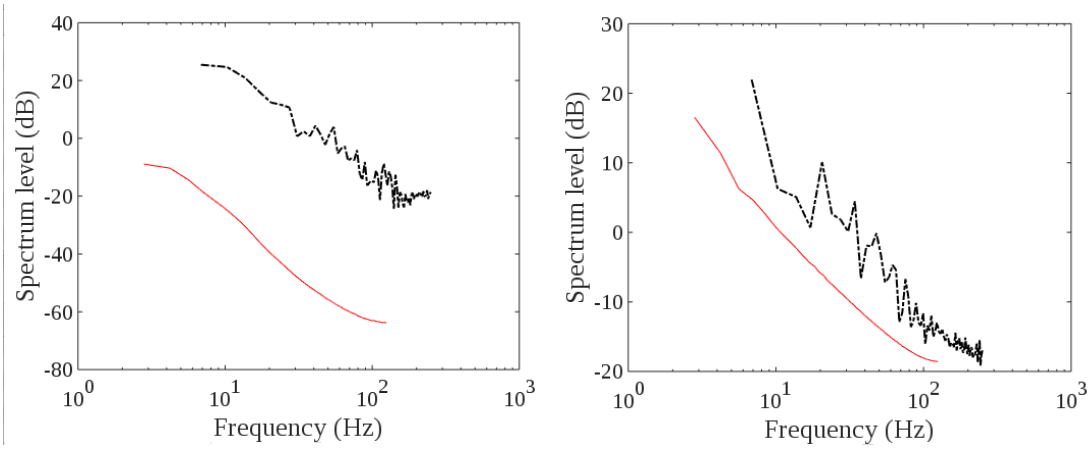

Figure 2: Comparison of linear terms (left panel) and nonlinear terms (right panel) of the FW-H reconstructed signal in the frequency domain, at a distance of $100D$*. Case of a flow around a sphere (black dashed line) and a prolate spheroid (red solid line).*

3.3.2. Cube vs square cylinder

This section is devoted to a qualitative comparison between the hydroacoustic field generated by a cube and an elongated cylinder with a squared section. The different aspect ratios, 1 for the cube and 30 for the cylinder respectively, make the difference. In fact, the elongated object releases von Karman vortex sheet, while, the cube generates a short wake, which appears disordered and strongly three-dimensional.

In Figure 3, the contour of the streamwise velocity component shows this difference: the flow downstream the cylinder (right panel) is characterized by the presence of a persisting and oscillating wake, which becomes progressively wider and finally breaks, turning into a rather chaotic and turbulent flow; the wake behind the cube (left panel) is more irregular and, above all, spreads out much sooner in the field, thus providing a much weaker occurrence of nonlinear noise sources in a spatially limited region.

The FWH reconstructed signal is in Figure 4, FWH linear terms contribution on the left panel and FWH nonlinear terms contribution on the right panel. The FWH linear terms generated by

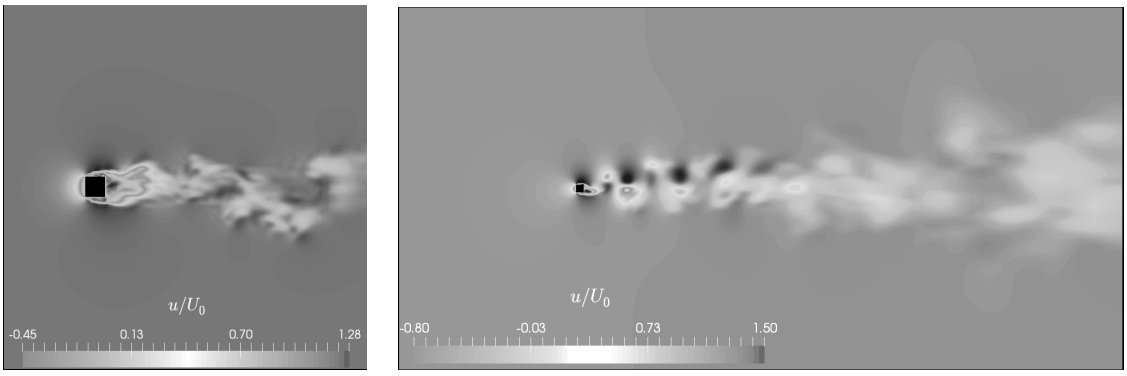

Figure 3: Comparison of instantaneous streamline velocity u, made non-dimensional by the inlet uniform velocity U_0, in the case of flow around a cube (left panel) and flow around a square cylinder (right panel). The Figure was taken from [11].

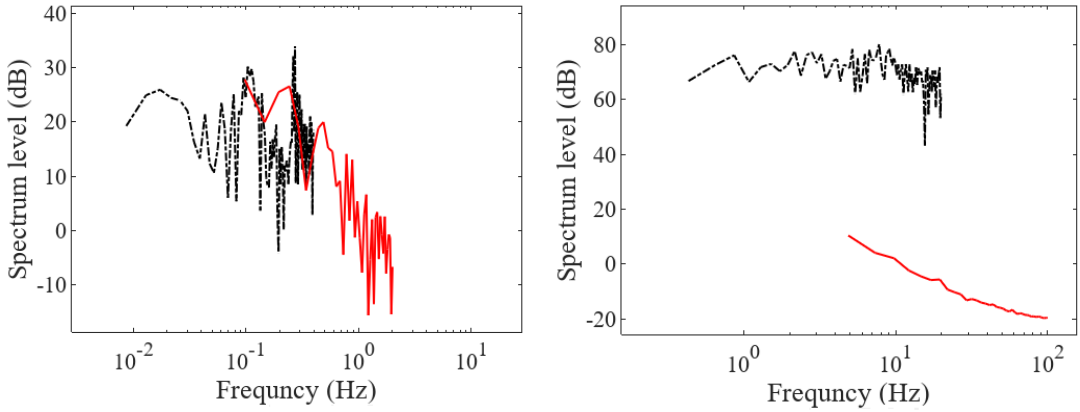

Figure 4: Comparison of linear terms (left panel) and nonlinear terms (right panel) of the FW-H reconstructed signal in the frequency domain, at a distance of $100D$*. Case of a flow around a square cylinder (black dashed line) and a cube (red solid line).*

the cylinder show a peak at a very low frequency caused by the alternating vortex released, its amplitude being comparable with that of the cube linear terms, about $20 - 30\,dB$. However, as expected the loading pressure on the cube produces a more complex and broadband spectrum (black dashed line on the left panel of Figure 4), due to the impact of the flow with the four sharp corners. The nonlinear part (panel on the right) in the two cases behaves in a different way. The cube behaves similarly to the sphere, shown in the previous subsection, while the noise generated by the cylinder wake is considerably higher (about $50\,dB$) and richer.

4. ISOLATED MARINE PROPELLER

We consider a benchmark propeller, the SVA VP1304, whose complete documentation, including geometry and experimental and numerical data, is available at the website https://www.sva-potsdam.de/en/potsdam-propeller-test-case-pptc.

4.4.1. Numerical setup

In the present study, we show results for the uniform flow case of the isolated propeller, at design advance ratio and Reynolds number respectively:

$$J_v = \frac{U_{0x}}{nD} = 1.0683, \quad Re = \frac{U_{0x}D}{\nu} = 889\,680, \tag{6}$$

where $U_{0x} = -4\ m/s$ is the advance velocity along the x-direction, n is the rotational velocity in rps and $D = 0.25\ m$ the diameter of the propeller.

For the value $J_v = 1.0683$, the thrust (K_T) and torque (K_Q) coefficients are:

$$K_T = \frac{S}{\rho n^2 D^4} = 0.3538, \qquad K_Q = \frac{Q}{\rho n^2 D^5} = 0.09096, \tag{7}$$

where S and Q are the thrust and the torque provided by the propeller.

The rotation direction of the five-blade propeller is right-handed. We use a cylindrical numerical domain, as sketched in 5; the diameter is equal to $7D$, and the length is $10D$ as suggested in [4]. The reference coordinate system is chosen such that the blades of the propeller are located at the plane $x = 0$ and the flow is in the direction of negative x. A cylindrical O-grid is created not uniform along the streamwise direction. The cells are clustered in the regions occupied by the hub and the blades and coarsened moving towards the lateral boundaries. Then the OpenFoam tool SnappyHexMesh is adopted to merge the propller geometry within the cylindrical grid. The grid is composed of about 6 millions cells, the mesh quality parameters fit the OpenFoam criteria of aspect ratio, skewness and non-orthogonality. The near wall resolution is such to obtain a distance of the first grid point off the wall of about 13.6 y^+. A wall-layer model is adopted and is described in detail in [11].

As boundary conditions, at the inlet section we give a uniform flow field U_{0x}, at lateral boundaries we set a slip condition and at the outlet the outflow we impose a zero gradient condition. At the solid walls of the shaft, hub and blades, the tangential velocity is imposed based on $u_t(r) = \bar{\Omega}\times\bar{r}$, with $\bar{r}$ radius from the rotation axis, and $\bar{\Omega} = (2\pi n, 0, 0)$, with $n = 15\ rps$. For the pressure, we set $\partial p/\partial n = 0$ to all boundaries of the computational domain, n being the direction normal to the surface. The constant flow density and the speed of sound are set $\rho = 998\ Kg/m^3$ and $c_0 = 1400\ m/s$ respectively, these quantities being necessary for the acoustic analysis.

After the field has completely developed, completing about 60 complete revolutions, data were collected for about 5 revolutions after that a statistically steady state had been reached. The time step of the LES is $dt = 10^{-6}\ s$ corresponding to a Courant number less than 0.5 and the flow field, pressure p and velocity U, are printed out every $dt_p = 0.0027\ s$ (which correspond to about 15 degrees).

For the value of the advance coefficient $J = 1.068$ we obtain the following values of the force and torque coefficients: $K_{T_s} = 0.3650$ and $K_{Q_s} = 0.09277$ corresponding to errors of $e_{K_{T_s}} = 3.18\%$, and $e_{K_{Q_s}} = 1.89\%$, with respect to experimental data.

The coefficients are reproduced satisfactorily; in previous studies (see for example [12]) concerning wall-modeled LES, thrust and torque coefficients were obtained within an error of 5% with respect to the reference experimental values.

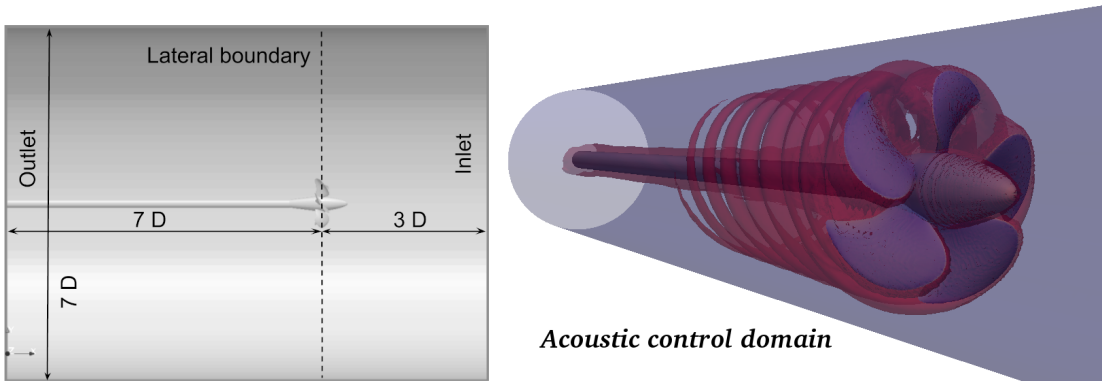

Figure 5: Computational fluid dynamic domain and acoustic domain.

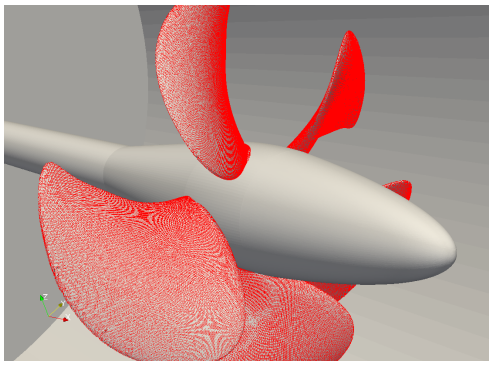

Figure 6: Retarded surface Σ together with solid surface.

4.4.2. Acoustic analysis of the propeller

In presence of an immersed moving body, such as a rotating propeller, a consideration on the importance of time delays can be addressed by calculating the retarded surface Σ (see [1]). Σ is the surface constituted by the points $y(\tau)$, such that. $t - \tau - |\mathbf{x} - \mathbf{y}(\tau)|/c_0 = 0$. In this case the observer $\mathbf{x}$ is immobile and the source $\mathbf{y}$ rotates over time. At low rotational Mach numbers, as those typical of ship propellers, the retarded surface coincides with the propeller surface, as depicted in Figure 6 for the case herein investigated: gray surface is the solid surface and red wireframe is the Σ surface. Thus, impulsive pressure signals scattered from the propeller surface reach the observer at the same time, meaning that, they do not add up each other over time. In this case, direct integration of kernels is allowed without the need to consider the time delays computation.

Two measurement points are selected: microphone A on the propeller plane $x = 0$, at distances 0.6 D from the axis of rotation, thus just out of the tip of the blades; microphone B at the same distances 0.6 D from the axis of rotation, but moved downstream at $x = 1D$. When computing the FWH integral volume terms, we adopted a cylindrical acoustic control domain, as depicted in Figure 5, in order to include the entire wake contribution.

The spectrum signal, expressed in a logarithmic scale, is reported in Figure 7 for microphone A (left panel) and B (right panel). We recall that the Sound Spectrum Level is evaluated as

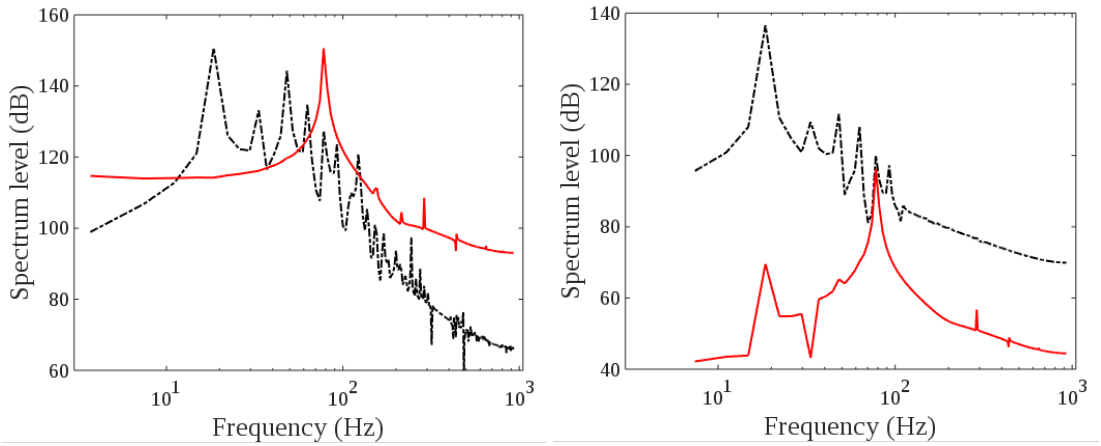

Figure 7: Spectrum level evaluated at michrophone A (left panel) and microphone B (right panel). FWH linear terms (red solid line) and FWH non linear terms (black dashed line).

$SPL = 20\log_{10}(A/p_{ref})\ dB$, being A the amplitude of the signal and $p_{ref} = 1\ \mu Pa$ the reference pressure for underwater measurements. The signature of the linear terms is strongly periodic (see the red line in both panels of Figure 7), with a frequency equal to nN, being n the number of revolutions per second and N the number of blades. Very close to the propeller (microphone A) the amplitude peak reaches about 150 dB, while moving dowstream the tonal noise level decreases to 100 dB. The frequency analysis clearly shows the contribution of the quadrupole terms in the range of low frequencies. The main peak is at about $15 - 20\ Hz$, in correspondence of the revolution frequency n and other peaks are sub-harmonics of the blade frequency nN. To be noted that the quadrupole, nonlinear term significantly contributes at both locations. Also, comparatively, it contributes more to the overall noise, with respect to linear terms, at microphone B which is farther than A from the propeller. In other words, the rate at which the signal associated to the nonlinear terms decrease with distance is slower than that of linear terms.

The reason is that the peak on the low frequency n is given by the shaft vortex, which persists on wake. To make this point clear, we show in Figures 8 an instantaneous snapshot of vorticity magnitude isosurface $|\omega| = 100$ together with contour of the scalar quantity $\partial^2 T_{ij}/\partial x_i \partial x_j$. The latter is related to the Lighthill tensor of FWH equation, which constitutes the instantaneous nonlinear (in terms of velocity field) source of the acoustic wave equation.

The figure shows that the most energetic contribution to the Lighthill tensor and thus to the non-linear source of noise may be the energetic helical vortex that forms around the propeller shaft. This vortex structure appears even more significant than the tip vortex. Also, its spatial distribution, specifically the distance between two successive vortexes along the mean flow direction, is consistent with the low frequency observed in the SPL. In literature it is often observed as hub vortex, since the mean flow direction is oriented along the opposite direction to the shaft (so here it would be for positive x). The frequency associated to the shaft vortex is consistent with that expressed in previous works, see for example [13] who reported that the wave number associated to the shaft vortex is $1/N$ times that associated to the tip vortex.

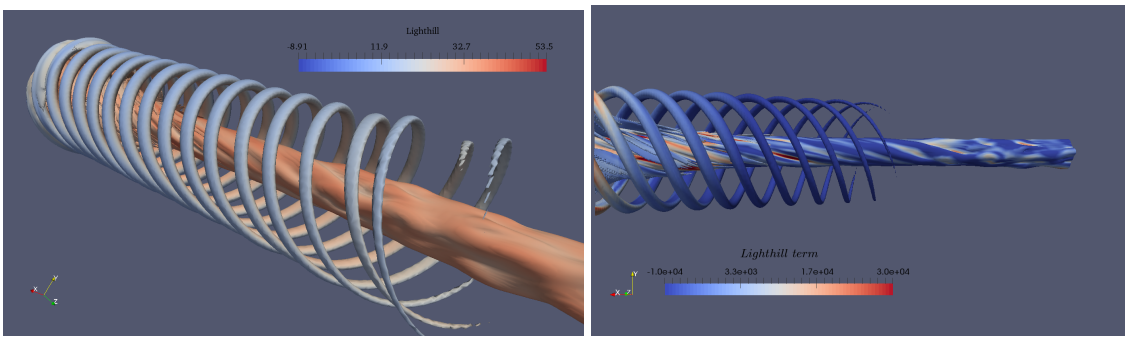

Figure 8: Isosurface of vorticity magnitude $|\omega| = 100$ *(left panel) and* $|\omega| = 200$ *(right panel). Contour of scalar term* $\partial^2 T_{ij}/\partial x_i \partial x_j$*, related to the Lighthill tensor of FWH equation.*

5. CONCLUSIONS

In the present study we adopted the Ffowcs Williams and Hawkings analogy to characterize the noise source, in case of a marine propeller.

The first part of the manuscript is dedicated to the summary of some results obtained in the first stage of the research. Specifically, first different solution methods were assessed, successively the FWH method was applied on simple cases, of flow around bluff bodies, and finally, we analysed the noise from of a ship propeller. As regards the methodology, our research clearly shows that, in hydrodynamics, the direct integration of the quadrupole volume terms composing is feasible and provide accurate results, provided that a criterion based on the MFP parameter is satisfied. The study of the acoustic field generated by elementary geometries allowed to understand the effect of massive separation and three-dimensional wakes on the generation and propagation of noise. In particular, a fully 3D wakes is less noisy than a 2D wake, as those generated around slender bodies. Also, bluff bodies generating massive separation appear more noisy than slender streamlined geometries. Finaly, the study of a marine propeller in open water shows that the wake together with the shaft vortex provide a significant contribution to the overall noise.

6. ACKNOWLEDGEMENTS

This work was supported by Region FVG-POR FESR 2014-2020, Fondo Europeo di Sviluppo Regionale, Project PRELICA *Metodologie avanzate per la progettazione idroacustica dell'elica navale*.

7. REFERENCES

[1] Ianniello S., Muscari R. and Di Mascio A. *Ship underwater noise assessment by the acoustic analogy. Part I: nonlinear analysis of a marine propeller in a auniform flow*. Journal of Marine Science and Technology, 18(4), pp. 547-570, 2013.

[2] Cianferra M., Ianniello S. and Armenio V. *Assessment of methodologies for the solution of the Ffowcs Williams and Hawkings equation using Large-Eddy Simulations of incompressible single-phase flow around a finite-size square cylinder*. Submitted.

[3] Brentner K.S. and Farassat F. *Modeling aerodynamically generated sound of helicopter rotors*. Progress in Aerospace Sciences 39, 2-3, pp. 83-120, 2003.

[4] Kumar P., Mahesh K. *Large eddy simulation of propeller wake instabilities*. J. Fluid Mech., vol. 814, 2017.

[5] Meneveau C., Lund T.S. and Cabot W.H. *A Lagrangian dynamic subgrid-scale model of turbulence*. J. Fluid Mech., vol. 319, p. 353-385, 1996.

[6] Cintolesi C., Petronio A. and Armenio V. *Large-eddy simulation of thin film evaporation and condensation from a hot plate in enclosure: first order statistics*. Int. J. Heat Mass Transf. 101, 1123, 2016.

[7] Cintolesi C., Petronio A. and Armenio V. *Large eddy simulation of turbulent buoyant flow in a confined cavity with conjugate heat transfer*. Phys. Fluids 27, 2015.

[8] Najafi-Yazdi, A., G.A.Bres, Mongeau, L. *An acoustic analogy formulation for moving sources in uniformly moving media*. Proc R Soc Lond A467, 144–165, 2011.

[9] Cianferra M., Armenio V. and Ianniello S. *Hydroacoustic noise from different geometries*. Accepted on Int J Heat Fluid Fl, Available online 22 December 2017, In Press.

[10] Ianniello S., Muscari R. and Di Mascio A. *Ship underwater noise assessment by the acoustic analogy. Part II: hydroacoustic analysis of a ship scaled model. Journal of Marine Science and Technology*. 19 (1), pp. 52-74, 2014.

[11] Cianferra M., Petronio A.. and Armenio V. *Hydrodynamic noise from an isolated propeller*. Proceeding paper NAV2018 Conference, 2018.

[12] Di Felice F., Felli M., Liefvendahl M. and Svennberg U. *Numerical and experimental analysis of the wake behavior of a generic submarine propeller*. In First International Symposium on Marine Propulsors, Trondheim, Norway 2019.

[13] Felli M., Camussi R. and Di Felice F. *Mechanisms of evolution of the propeller wake in the transition and far fields*. J. Fluid Mech., pp 1 - 49, 2011.